

Deposition of $\text{La}_2\text{Zr}_2\text{O}_7$ Film by Chemical Solution Deposition

Z.M. Yu¹, P. Odier^{2,3,*}, S. Morlens^{2,3}, P. Chaudouët^{3,4}, M. Bacia⁴, L. Zhou¹, P.X. Zhang¹, L.H. Jin¹, C.S. Li¹, P. David², O. Fruchart², Y.F. Lu¹

1. Northwest Institute for Nonferrous Metal Research, P.O.Box 51, Xi'an, Shaanxi, 710016, P.R.China

2. Néel Institut, CNRS&UJF, 25 avenue des Martyrs, BP166, 38042 Grenoble Cedex, France.

3. CRETA, CNRS, 25 avenue des Martyrs, BP166, 38042 Grenoble Cedex, France.

4. Laboratoire des Matériaux et du Génie Physique - BP 257- INPGrenoble Minatec - 3 parvis Louis Néel - 38016 Grenoble – France.

* Corresponding author: P. Odier, philippe.odier@grenoble.cnrs.fr, Néel Institut (département MCBT, bât.E)/CRETA (Bât. V), CNRS, 25 av des martyrs, BP 166, F-38042 Grenoble cedex 09, France, tel: (33) (0)4 76 88 90 34, fax: (33) (0)4 76 88 12 80.

Abstract

$\text{La}_2\text{Zr}_2\text{O}_7$ (LZO) formation of bulk powders and of films by Chemical Solution Deposition (CSD) process have been studied using propionates. The treatment involved a one step cycle in the reducing forming gas (Ar-5\%H_2) to be compatible with Ni-5at%W RABITS. Large amount of residual carbon was found in LZO powders formed in these conditions (10 wt %). The volume fraction of the cube texture in LZO films on Ni-5at%w RABITS was found to be a function of the speed of the gas flown above sample. This phenomenon is discussed in considering the C deposited from the carbon-containing gases emitted during the pyrolysis of the precursor. Using proper conditions (950 °C and the speed of gas of 6.8×10^{-2} m/s), LZO films with good surface crystallinity could be obtained on Ni-5at%W RABITS as demonstrated by X-ray diffraction, electron backscattered diffraction and RHEED. The existence of residual carbon in oxide films is a common question to films deposited by CSD processes under reducing condition.

Keywords: chemical solution deposition; MOD; oxide; $\text{La}_2\text{Zr}_2\text{O}_7$; film; texture

1. Introduction

1 The second generation of high-temperature superconducting tapes, also named
2 $\text{YBa}_2\text{Cu}_3\text{O}_7$ (YBCO) coated conductors (CCs), sustains a considerable interest and many
3 challenges in the material science community [1]. YBCO is very anisotropic and needs to be
4 cube-textured along its principal axes ([001] and [100]) to allow high superconducting
5 currents across its grain boundaries [2]. The CCs tapes must be flexible for their assembling
6 into cables used in electricity transportation [3]. Films technologies to deposit YBCO layer on
7 a flexible metallic substrate only permit to fulfil these constrains. Ni rolled assisted bi-axially
8 textured substrates (RABITS) are attractive substrates [4], but several buffer layers between
9 the metallic substrate and the YBCO layer are very important because almost all of metallic
10 elements in the metallic substrate are harmful to the superconductivity of YBCO layer. Quite
11 complex architectures of buffer layers have been successfully used on NiW alloys such as
12 those developed by American Superconductors [4] or others.

13 LZO is a highly refractory oxide (high melting point over 2200°C) and shows interesting
14 properties in radiation tolerance [5], ionic conductivity [6] in doped compositions, thermal
15 barrier coating [7]. Besides these application fields, LZO is also an important material to be
16 used for buffer layers. The simplest low cost architecture with only one buffer made of
17 $\text{La}_2\text{Zr}_2\text{O}_7$ (LZO) has been recently validated using an original combination of chemical
18 methods involving metalorganic chemical vapour deposition (MOCVD) and metal organic
19 decomposition (MOD); i.e. $\text{YBCO}_{\text{MOCVD}}/\text{LZO}_{\text{MOD}}/\text{NiW}_{\text{RABITS}}$ [8].

20 Cost, scalability and simplicity of process are essential ingredients to be considered for
21 long-length CCs tape production. Chemical solution deposition (CSD) is very attractive in
22 this respect and much used for functional oxide films synthesis [9, 10] in three principal
23 approaches: sol-gel, metal-organic decomposition (MOD) and hybrid routes. Sol-gel uses
24 controlled hydrolysis-condensation reactions to build up a 3D organic-inorganic network [11],
25 MOD consists in pyrolysing a metal-organic precursor after its drying into a dense glaze
26 followed by its crystallisation. MOD is often preferred to prepare epitaxial films because the
27 3D network has been suspected to be detrimental to epitaxial growth [12]. However MOD
28 needs a fine control of the decomposition step and for its crystallisation into oxide, both
29 transformations which are complex to study.

30 Several important works have been done to deposit LZO films for buffer layers by CSD
31 approaches [13, 14, 15]. However, the reactions leading to the formation of LZO are not
32 clearly established yet as stress the following, but non exhaustive, list of open questions. *First*,
33 the precursor structure itself is often unknown while it might influence the molecular mixing
34 at a local level with a possible influence on the microstructure. *Second*, the pyrolysis of the
35
36
37
38
39
40
41
42
43
44
45
46
47
48
49
50
51
52
53
54
55
56
57
58
59
60
61
62
63
64
65

precursor must be conducted under Ar-5% H₂ to avoid any oxidation of the metallic substrate, then reduction of the evolved molecules can be anticipated with important consequences on the crystallisation of the oxide. C deposit has been observed by Rutherford back scattering [14] in such a process (depending however of the forming atmosphere); C could play an important role in the growth [16] and in the build up of the microstructure as observed in a similar case [17, 18]. C was removed efficiently by adding humidity in the forming gas (Ar-5 % H₂) but this destroyed the texture [14] ((222) orientation grains were enhanced and (400) decreased). *Third*, while the texture of LZO films obtained on Ni-5at%W substrates reproduces very well that of the substrates [8, 19, 20], the exact mechanism of epitaxy is still an open question [21] since a high structural mismatch ($(\epsilon_{LZO}-\epsilon_{Ni})/\epsilon_{Ni} \sim 8\%$) exists with the substrate. However, it is reasonable to admit that the nucleation starts at the interface with the substrate. This is supported by the fact that, at 800 °C, LZO was observed strongly c-axis textured by X ray diffraction (XRD) but amorphous at its surface according to surface probing by reflexion high energy electron diffraction (RHEED); it became bi-axially textured up to its surface after annealing at 900 °C or above [15]. The crystallisation has started at the metal/oxide interface and has developed at higher temperature by growing within the amorphous volume of the film up to its surface. *Fourth*, the microstructure shows rather peculiar properties. Polygonal nanovoids have been identified by transmission electron microscopy (TEM) [21], suspected but not discussed in Ref. 22, and recently studied in more details by TEM [23]. These nanovoids play an important role since they reduce the effective length of matter protecting the metallic substrate from oxidation during the deposition of YBCO [8]. It is clear from this list that even if LZO buffers with excellent properties are actually produced by MOD [24] in a continuous line, many important questions remain unsolved in relation to the MOD process applied to LZO films.

In this research we aimed to study in details the role of the atmosphere on the crystallisation of LZO films deposited on Ni- 5at% W substrates from propionate solutions by spin coating. We used a cycle with one thermal step in which the pyrolysis was not treated separately from the crystallisation. The goal was to increase the crystallised part of the film, and to improve its texture. During the course of this research, we have also studied the reaction synthesis of LZO powders in order to provide some information on the crystallisation mechanism of bulk LZO.

2. Experimental

Lanthanum(III) 2,4-pentanedionate (La(acac)₃·3H₂O) and zirconium(IV) 2,4-pentanedionate (Zr(acac)₄) were used as solute. After weighing, a stoichiometric mixture of

1 La(acac)₃ and Zr(acac)₄ was introduced into propionic acid. The solution was placed in an
2 ultrasonic bath for 15 min, then stirred and heated at 60 °C for 30 min. Finally, a transparent
3 yellow precursor solution was obtained [25]. The concentration of the precursor solution was
4 0.5 mol/L (with respect to La³⁺).
5

6 The precursor solution was dried at 100 °C to remove the solvent, yielding a dry
7 precursor powder which was named hereafter the “as-received” powder. As-received powders
8 were heat-treated at different temperatures for 30 min under Ar-5% H₂ atmosphere with the
9 same heating rate (850 °C/h), the flow of gas was fixed at 0.5 l/h by a flow-meter. The
10 structure of black residual powders was checked by x-ray diffraction (XRD), TEM (Philips
11 300 CX) and their chemical composition was also analyzed. Chemical analysis was
12 performed on small samples (10-100 mg) at the central analysis centre of CNRS (CNRS-
13 Vernaison Lyon, France). Metallic elements were determined by ICP in solution (with a
14 relative error of 2%), C and H were quantified by catharometric detection (relative error
15 0.3 %), O was determined by measuring CO₂ produced by reaction of the pyrolysed products
16 on an active C.
17

18 Ni-5%W substrates (size: 5 mm × 5 mm) were cut from a long tape (Evico GmbH),
19 cleaned by acetone for 10 min in an ultrasonic bath, and covered by the precursor solution
20 using spin-coating (rotation speed: 2500 rpm, rotation time: 30 s, acceleration: 3000 rpm/min),
21 then the samples were dried at 80 °C for several minutes in air. _____
22

23 ~~All the~~ _____
24 samples were heated at 950 °C for 30 min under Ar-5% H₂ flow with a fixed heating rate of
25 850 °C/h. The films' thicknesses were measured by profilometry and by fitting the IR
26 reflectivity. The films' thicknesses were typically in the range of 50-100 nm. Besides Ni-
27 5at%W substrates, LaAlO₃ (100) single crystals (LAO) were also used in particular cases.
28

29 The texture of all samples was characterized by x-ray diffraction using a four-circle
30 diffractometer (Siefert MZ IV) in the Schulz configuration. The diffractometer worked at Cu
31 K_α wavelength with collimating multilayer optic from Xenocs (Grenoble, France) enabling a
32 low divergent beam (horizontal angular divergence was 0.06° and the vertical one was 0.1°)
33 with an irradiated area covering 2x1 mm². A graphite analyzer is mounted before the detector
34 to prevent parasitic photon collection. This device is very efficient for measuring texture or
35 studying single crystals or epitaxial thin films. In particular it has a very high signal/noise
36 ratio enabling to detect diffracted peaks with weak intensities in the range of a few counts per
37 second (c/s). Due to these intrinsic characteristics the diffracted intensity on polycrystalline is
38 divided by 5 to 10 compared to more conventional apparatus (like D5000 Siemens in Bragg-
39
40
41
42
43
44
45
46
47
48
49
50
51
52
53
54
55
56
57
58
59
60
61
62
63
64
65

Brentano scheme). Therefore, the reader must not be surprised by the low intensities recorded during this research. The crystalline quality of the surface of LZO films was checked by electron back scattered diffraction (EBSD) and RHEED.

XPS has been used to study the residual C at the surface of the films. The apparatus was a Axis Ultra from Kraos analytical Ltd. (GB). C (1s) has been registered versus sputtering time in the binding energy range 272-292 eV. The sputtering was performed with Ar ions accelerated at 4 kV under 15 mA providing a sputtering rate in the range of 0.1-0.2 nm/min.

3. Results

3.1 Synthesis of bulk LZO powder under a reducing atmosphere

Part of the as-received powders was heat treated under Ar-5% H₂ flow at 500 °C, 700 °C, 900 °C and 1100 °C to study its chemical composition evolution by chemical analysis and its crystallisation by XRD and by TEM.

The results of chemical analysis are reported in Table 1. Starting from a pentadionate precursor, it is obvious that the as-received powder was closer to a propionate than to a pentadionate. It agrees with the transformation occurring during their dissolution into a solution as already mentioned [15, 25]. During the heat treatment, H is completely eliminated while substantial amounts of C and O remain. The remaining oxygen points to the formation of an oxide; i.e. La₂Zr₂O₇ (LZO), as is certified by the weight loss analysis corresponding at 1100 °C to within 2% to the nominal composition of this oxide [25] when C is not taken into account in the molar fraction of the residue at 1100°C. The overall residual C level is very high, amounting 12 wt% even after heating at 1100 °C. Such large amount of carbon would correspond to approximately 6.6 mole of C per one mole of LZO. It should be noticed that the proportion of C increased slightly with heating due to the removal of H and O species during the conversion of the as-received powder into LZO.

XRD was performed on the heat treated powders, Fig. 1a. At 700 °C the powder was mainly amorphous with a unique diffracted peak at the position of the (111) peak of the fluorite form of LZO (SG Fm-3m, according to ICSD28991 data file). At 900 °C most of the peaks of the fluorite phase were visible. At 1100 °C all the peaks were indexed within the pyrochlore unit cell (SG Fd-3m according to ICSD15165). It means that the crystallisation of LZO powder from propionate precursor occurs in the temperature range 700-900 °C, that agrees well with what was found in films on Ni-5at%W substrates (800-850 °C) [13, 14, 15]. The structure of the oxide undergo a transformation from the fluorite phase to the pyrochlore phase at higher T, i.e. between 900 °C and 1100 °C. The fluorite phase is disordered and metastable in this temperature range [5].

1 TEM observations on these heat-treated powders confirmed that the onset of
2 crystallisation of the as-received powder was at 700 °C, fig.1b. Some grains were already
3 crystallised, and the electron diffraction pattern from a selected area confirmed that these
4 grains were LZO. Fig.1c shows a TEM image of several grains after heating at 950 °C. All
5 these grains had well organised facets and atomic planes in many grains were visible,
6 testifying an almost complete crystallization. The mean grain size remains small, i.e. <10 nm.
7 At 1100 °C, fig.1d, the TEM image shows that the grains had grown a little compared to
8 grains synthesized at 950 °C, reaching about 10 nm while sintering has already started leading
9 to large agglomerates (several hundreds of nm).

15 3.2 Deposition of LZO film

17 In a preliminary study, LZO films were deposited on LaAlO₃ (LAO) single crystals and
18 heat treated at 950 °C for 30 min under air or Ar-5% H₂ flow. The case of air treatment is
19 presented first. Except the reflexions from the substrate, the only diffracted lines in a θ - 2θ
20 diagram (Fig.2a) were observed at $2\theta = 33.20^\circ$ and 69.8° (not shown). This is a
21 characteristic of a strongly c axis oriented LZO film. The (111) and (200) pole figures (not
22 shown) proves the epitaxial nature of the film. Its structure may be fluorite or pyrochlore, the
23 later one being characterised by {331} planes that are absent in the fluorite structure. The pole
24 figure analysis of the {331} reflections evidencing 8 reflections at the tilt angle of $\chi = 46.5^\circ$
25 due to (331) and equivalents and 4 reflections at $\chi = 76.7^\circ$ due to (133) and equivalents, fig.
26 2b, demonstrates that the structure of this film is pyrochlore. So the peak at $2\theta = 33.20^\circ$ was
27 indexed as (400) relative to the pyrochlore phase of LZO.

28 The diffracted intensity of the (400) peak of the samples which were heat treated under
29 air flow is every high; surprisingly, the peak intensity dropped by a factor 5 to 10 when the
30 atmosphere was switched to a reducing atmosphere (Ar-5%H₂). It indicates a less efficient
31 crystallisation under very low oxygen partial pressure. In the case of a reducing atmosphere,
32 the oxygen in the atmosphere surrounding the sample was due to residual leakage of the
33 furnace and was measured by a mini zirconia gauge (from SETNAG-Marseille France)
34 installed directly above the sample. At 950 °C the oxygen partial pressure was in the range of
35 10^{-20} atm. Curiously, under Ar-5%H₂, the diffracted intensity was sensitive to the speed of the
36 gas flown over the sample and the line shifted to higher angle ($2\theta = 33.38^\circ$) indicating a
37 deformed structure of LZO. The intensity increased by a factor of 2 when the speed of the gas
38 was increased from 1.2×10^{-4} m/s to 2.2×10^{-3} m/s. The speed of the gas was approximated by
39 the flow (imposed by a flow meter) divided by the section of the tube. In order to know if this
40 phenomenon was linked with the crystallisation of LZO or with an effect of the substrate,
41
42
43
44
45
46
47
48
49
50
51
52
53
54
55
56
57
58
59
60
61
62
63
64
65

several experiments were performed on Ni-5at%W substrates which are used in CCs applications.

Figure 3 shows the effect of the gas forming speed on the diffracted intensity of six films of LZO deposited as single layer on Ni-5at% W substrates. The samples were heat treated under the same conditions except that the speed of gas was changed by modifying the set point of the flow meter. The samples were measured using same parameters of the diffractometer enabling to record quite reproducibly the diffracted intensities (on identical samples, the measured intensities varies less than 10 %). All these ensure an authentic comparison of the samples. The first observation concerns the diffracted intensities which were small, much smaller than the one obtained on LAO single crystals (several tenths). It may suggest the influence of an inhibiting factor on the growth. Secondly, the LZO films were strongly c axis textured but with random contributions evidenced by the (222) diffracted line when the speed of gas was lower than 2.2×10^{-3} m/s. Thirdly, the intensity of the (400) peak increased with increasing the speed of the gas flow. The increase (5 times) is much larger than experimental errors. Fourthly, the (222) contribution became negligible if the speed of the gas was sufficiently large, i.e. above 1.1×10^{-3} m/s. Finally, the intensity of (400) peak just increases slightly when the speed of the gas is higher than 3.4×10^{-3} m/s.

The best sample was characterized by XRD pole figure and EBSD which probes the sample's surface crystallinity. Fig. 4a shows the XRD pole figure of (222) which is a typical cube-textured LZO film grown epitaxially on the Ni-5at%W substrate. The epitaxial relationship is $[100]_{\text{Ni}} // [220]_{\text{LZO}}$ and $[001]_{\text{Ni}} // [001]_{\text{LZO}}$ as is usually observed by others. The in-plane rotation of LZO unit cell with respect to that of Ni is to better match both unit cells. Fig. 4b shows the same pole reconstructed from EBSD data. It clearly demonstrates that the surface of the film had the same texture. The sharpness of the texture was as good as that of the metallic substrate (typically 6.5° for in-plane texture, and 7.4° for out-of-plane texture). It is useful to mention that the RHEED pattern (Fig. 5) of this film also shows that the ultimate surface (1 nm) was textured. The spots had some tendency toward a ring-shaped elongation in connection with the angular misalignment between grains. The planar misalignment was estimated by RHEED in the same range as those measured by XRD. The surface was rough at a scale of a few nanometers from AFM. Obviously, the crystallinity of the best films was good and could serve as a template for the epitaxial growth of other oxide film.

The C content of the top layer of LZO/Ni5W films has been probed by XPS after sputtering with Ar ions at a low rate of 0.1-0.2 nm/min. Samples processed under large gas flow were compared to samples processed at low gas flow and two annealing temperatures were compared. The data are combined in Fig. 6 where the C at% (vertical axis) is estimated

1 from the photoelectron peak of C 1s (at 283 eV, binding energy), and the horizontal axis is the
2 sputtering time. The figure shows a rather large C concentration at the top layer of LZO (4-7
3 at %), even after a treatment at 950°C for 40 min. Increasing the annealing temperature from
4 800 °C to 950 °C has not a spectacular effect, while increasing the gas speed over the sample
5 decrease the surface C content. Even more, it shows that the C distribution is not
6 homogeneous when the gas flow is small which agrees with amorphous or not textured areas
7 in the depth of the sample.
8
9
10
11
12

13 **4. Discussion**

14
15 Measurements of the chemical composition of bulk powders treated under Ar-5%H₂ to
16 reproduce the conditions used for films synthesis showed a large amount of residual C (up to
17 12 wt %), trapped in the powder. Films of LZO also showed residual C at their surface but in
18 lower proportion; the content and distribution of C seems to be affected by the gas flow. It is
19 believed that this phenomenon is due to the heat-treatment atmosphere. Besides of our case,
20 the phenomenon has been found in other MOD films deposited by CSD process [17, 26].
21
22

23 It is believed that the residual carbon is due to the phenomenon of carbon deposition
24 which is well known in catalysts. The carbon deposition is an important reason for loss of
25 catalytic activity. In the case of the partial oxidation of methane to produce syngas [27],
26 authors discussed the possibility of decomposition of CO₂ or CH₄ to form carbon. In our case,
27 the decomposition of propionate precursors emitted carbon-containing gases, for example,
28 CO₂ or CH₄, and it is possible that these carbon-containing gases would be decomposed to
29 form solid carbon according to Ref. 27. Because the residual carbon results from the
30 decomposition of carbon-containing gases, and the decomposition of propionate precursors is
31 almost finished at 800 °C [25], this can explain the reasons why there was an amount of
32 residual carbon in final powders and why the amount of residual carbon changed slightly after
33 heating above 700 °C.
34
35
36
37
38
39
40
41
42
43
44
45
46

47 TEM observation showed that the residual carbon existed at boundaries of LZO grains
48 and not in LZO grains. The impurity in grain boundaries influences effectively the crystal
49 growth during deposition of oxide films by CSD [16-18]. Other group results indicate that the
50 residual carbon would influence the development of LZO film's texture. Usually, the free
51 energy variation for nucleation is inversely proportional to the square of undercooling;
52 therefore in chemical solution deposition process the crystallization driving force is very large
53 [9, 10]. Although heterogeneous nucleation occurs more easily than homogenous nucleation
54 and starts at the substrate-oxide interface, the homogenous nucleation may become
55 competitive if the front of the epitaxial part cannot migrate rapidly due to some inhibiting
56
57
58
59
60
61
62
63
64
65

1 factor. Based on this analysis, it is possible that some randomly oriented grains grew on the
2 top layer of LZO film though the Ni-5at%W substrate owns a good cube texture, and then the
3 texture of the final LZO film is cube texture with additional random orientations. Similar
4 result has been found by others [17, 26]. This group demonstrated that the bottom layer of
5 CeO₂ film deposited by CSD owned a cube texture while the top layer of the CeO₂ film could
6 be random due to the residual carbon. Hence, the deposition of residual C seems to be a
7 common phenomenon to CSD process when performed under reducing forming gas. It is
8 essential then to have an appropriate procedure for removing it in order to obtain a well
9 crystalline oxide film.

10 The main reason for the presence of residual carbon is the decomposition of carbon-
11 containing gases during the pyrolysis of the LZO precursor film, two routes can be imagined
12 to eradicate its influence. One is to increase the oxygen partial pressure to oxidize the residual
13 carbon, but it could result in oxidizing the Ni-5at%W substrate [28]; so only applying a
14 controlled oxygen partial pressure would be useful. We have preferred to use another simple
15 way by increasing the flow speed of Ar-5%H₂ to dissipate the carbon-containing gases as
16 rapidly as it can. The efficiency of this procedure has been demonstrated by our results (Fig.
17 3). According to knowledge about hydrodynamics, a boundary layer of C-containing gases
18 should always exist at the surface even for large applied gas speed. Then the effectiveness of
19 increasing the flow speed of Ar-5%H₂ gas has a physical limitation which has also been
20 proved by Fig. 3.

21 Based on the above-mentioned analysis, it is clear that the crystallisation and texture of
22 LZO films are dictated by two contributions, the epitaxial growth at the substrate/film
23 interface and the growth of the random part, if the treatment conditions are not optimized. The
24 LZO film with a well crystalline surface has been obtained when the carbon-containing gases
25 were dissipated as rapidly as possible.

26 V. Conclusion

27 LZO formation of bulk powders and of films by CSD process have been studied using
28 propionates treated in a reducing atmosphere (Ar-5%H₂). Large amount of residual carbon
29 was found in LZO powders formed in these conditions (10 wt %). It was left from
30 decomposition of carbon-containing gases emitted during the pyrolysis the precursor. Films of
31 LZO were deposited on Ni-5at%W RABITS. The volume fraction of the cube texture was
32 found to be a function of the speed of the gas flown above samples. Large speed of gas
33 promotes an efficient dissipation of the carbon-containing gases, and it was a good method to
34 eliminate the negative effect of the residual carbon in the crystallisation of LZO films. In
35
36
37
38
39
40
41
42
43
44
45
46
47
48
49
50
51
52
53
54
55
56
57
58
59
60
61
62
63
64
65

1 optimized deposition conditions, LZO films with good surface crystallinity could be obtained
2 on Ni-5at%W substrates. The existence of residual carbon in oxide films is a common
3 question to films deposited by CSD processes under reducing condition.
4
5

6 **Acknowledgements**

7
8 This work was supported by the French embassy in Beijing and the International
9 Laboratory for the Applications of Superconductor and Magnetic Materials (LAS2M-CNRS-
10 NIN). It was also supported by the National High Technology Research and Development
11 Program of China (863 Program) under contracts Nos. 2006AA03Z204 and 2008AA03Z202,
12 and French ANR-Madisup project. Drs L. Ortega and C. Jimenez (respectively at Néel Institut
13 and LMGP) are acknowledged for many helpful discussions. Drs De Sousa Meneses and B.
14 Rousseau at CEMTHI (Orléans-France) are acknowledged for thickness measurements by IR
15 reflectometry.
16
17
18
19
20
21
22
23
24
25
26
27
28
29
30
31
32
33
34
35
36
37
38
39
40
41
42
43
44
45
46
47
48
49
50
51
52
53
54
55
56
57
58
59
60
61
62
63
64
65

References

- 1
2 [1] A. Goyal (ed), *Second Generation of HTS conductors*, Kluwer Academic, Boston 2005.
3
4 [2] D. Dimos, P. Chaudari, J. Mannhart, F.K. LeGoues, *Phys.Rev.Lett.* **61** (1988) 219.
5
6 [3] <http://see.asso.fr/jicable/Workshops/WETS07>.
7
8 [4] A. Goyal, M. Paramanthaman, U. Shoop, *Mat. Res.Soc. Bulletin*, **29** (2004) 552.
9
10 [5] K. E. Sickafus, R. W. Grimes, J. A. Valdez, A.Cleave, M. Tang, N. Ishimaru, S. M. Corish,
11 C. R. Stanek, B. P. Uberuaga, *Nature materials*, **6** (2007) 217.
12
13 [6] M.A. Schubert, S. Senz, D. Hesse, *Solid State Ionics* **179** (2008) 453.
14
15 [7] Z. Xu, X. Zhong, J. Zhang, Y. Zhang, X. Cao, L. He, *Surface & Coatings Technol.* **202**
16 (2008) 4714.
17
18 [8] T. Caroff, S. Morlens, A. Abrutis, M. Decroux, P. Chaudouët, L. Porcar, Z. Saltyte, C.
19 Jimenez, P. Odier, F. Weiss, *Supercond.Sci.Technol.*, **21** (2008) 075007.
20
21 [9] R.W. Swartz, T. Schneller, R. Waser, *C.R. Chimie*, **7** (2004) 433.
22
23 [10] M.S. Bhuiyan, M. Paranthaman, K. Salama, *Supercond.Sci.Technol.*, **19** (2006) R1.
24
25 [11] J. Livage, M. Henry, J.P. Jolivet. *Inorganic polymerization in aqueous solution.*
26 *Chemical Processing of Advanced Materials* ed. by L.L. Hench and J.K. West, John Wiley &
27 Sons Inc., New York 1992.
28
29 [12] R.W. Schwartz, J.A. Voigt, B.A. Tuttle, D.A. Payne, T.L. Reichert, R.S. DaSalla, *J.*
30 *Mat.Res.*, **12**(2) (1997) 444.
31
32 [13] T G. Chirayil, M. Paranthaman, D B. Beach, D F. Lee, A. Goyal, R K. Williams, X. Cui,
33 D M. Kroeger, R. Feenstra, D T. Verebelyi, D K. Christen, *Physica C*, **336** (2000) 63.
34
35 [14] S. Sathiyamurthy, M. Paranthaman, T. Aytug, B.3 W. Kang, P.M. Martin, A. Goyal, D.M.
36 Kroeger, D.K. Christen , *J. Mater.Res.* **17**(6) (2002) 1543.
37
38 [15] K. Knoth, R. Hühne, S. Oswald, L. Schultz, B. Holzapfel, *Acta Materialia*, **55** (2007)
39 517.
40
41 [16] Nae-Lih Wu, Sze-Yen Wang, I A. Rusakova, *Science*, **285** (1999) 1375.
42
43 [17] F. Sandiumenge, A. Cavallaro, J. Gazquez, T. Puig, X. Obradors, J. Arbiol, H. C.
44 Freyhardt, *Nanotechnology*, **16** (2005) 1809.
45
46 [18] S. Engel, R. Hühne, K. Knoth, A. Chopra, N.H. Kumar, V.S. Sarma, P.N. Santhosh, L.
47 Schultz, B. Holzapfel, *J. Cryst. Growth* **310** (2008) 4295.
48
49 [19] E. Celik, Y. Akin, W. Sigmund, Y.S. Hascicek, *Materials Science and Engineering B*,
50 **106** (2004) 182.
51
52 [20] K. Knoth, R. Rühne, S. Oswald, L. Molina, O. Eibl, L. Schultz, B. Holzapfel, *Thin Solid*
53 *Films*, **516** (2008) 2099.
54
55
56
57
58
59
60
61
62
63
64
65

- 1
2
3 [21] L. Molina, K. Knoth, S. Engel, B. Holzapfel, O. Eibl, *Supercond.Sci.Technol.*, **19** (2006)
4 1200.
5
6 [22] M.P. Paranthaman, S. Sathyamurthy, M.S. Bhuiyan, P.M. Martin, T. Aytug, K Kim, M.
7 Fayek, K.J. Leonard, J. Li, A. Goyal, T. T. Kodenkandath, X. Li, W. Zhang, M.W. Rupich,
8 *IEEE Trans.on Appl.Sup.*, 17(2) (2007) 1051.
9
10 [23] L. Rapenne, C. Jiménez, T. Caroff, C. Millon, S. Morlens, P. Bayle-Guillemaud,
11 F.Weiss, *J. Mat. Res.* 24(4) (2009) 1480.
12 [24] M. O. Rikel, D. Isfort, M. Klein, J. Ehrenberg, J. Bock, E. D. Specht, M. Sun-Wagener,
13 O. Weber, D. Sporn, S. Engel, O. de Hass, R. Semerad, M. Schubert and B. Holzapfel, *IEEE*
14 *Trans. on Appl.Supercond.* **19** (2009) 3307.
15
16 [25] Z.M. Yu, P. Odier, L. Ortega, L. Zhou, P X. Zhang, A. Girard, *Mat. Sci. and*
17 *Engineering B*, **130** (2006) 126.
18
19 [26] M. Coll, J. Gazquez, F. Sandiumenge, T. Puig, X. Oradors, J.P. Espinos, R. Huhne,
20 *Nanotechnology*, 19 (2008) 395601.
21
22 [27] Q. G. Yan, T. H. Wu, J. T. Li, C. R. Luo, W. Z. Weng, L. F. Yang, H. L. Wan, *Journal of*
23 *Natural Gas Chemistry*, 9(2) (2000) 92.
24
25 [28] K.T. Jacob, *J.Mat.Sci.* **12** (1977) 1467.
26
27
28
29
30
31
32
33
34
35
36
37
38
39
40
41
42
43
44
45
46
47
48
49
50
51
52
53
54
55
56
57
58
59
60
61
62
63
64
65

Table caption

Table 1 Elemental analysis of “as-received” LZO powders and of the fired powders after treatments at increasing temperatures under Ar-5%H₂ flow, with a corresponding gas speed of 1.2×10^{-4} m/s. Nominal weight fractions for propionate and pentadionate are indicated for comparison.

1
2
3
4
5
6
7
8
9
10
11
12
13
14
15
16
17
18
19
20
21
22
23
24
25
26
27
28
29
30
31
32
33
34
35
36
37
38
39
40
41
42
43
44
45
46
47
48
49
50
51
52
53
54
55
56
57
58
59
60
61
62
63
64
65

Figures caption

1
2
3 Fig. 1 Crystallisation of bulk powders of LZO heat treated at different temperatures under Ar
4 - 5% H_2 gas flow: a) XRD; b) TEM of a powder heated at 700°C; c) id at 950°C: d) id at
5 1100°C. White scale: 10 nm.
6
7

8
9
10 Fig. 2 XRD of LZO films crystallised at 950°C on LAO under static air or Ar-5% H_2 flowing
11 at different speeds over the samples: a) XRD at tilt angle $\chi = 0$; b) pole figure evidencing the
12 pyrochlore structure of LZO with 12 {331} equivalent reflections expected. Three reflexions
13 are visible at $\chi = 76.7^\circ$, and seven at $\chi = 46.5^\circ$. The two missing reflections are barely visible
14 at $\chi = 46.5^\circ, \phi = 252^\circ$ and $\chi = 76.7^\circ, \phi = 252^\circ$ respectively.
15
16
17
18
19
20

21 Fig. 3 XRD of LZO films deposited on Ni-5at%W, treated at 950°C under Ar-5% H_2 gas flow
22 at different speeds of gas.
23
24
25

26 Fig. 4 XRD and EBSD pole figure on the best sample processed at the highest speed of gas
27 (6.8×10^{-2} m/s).
28
29
30

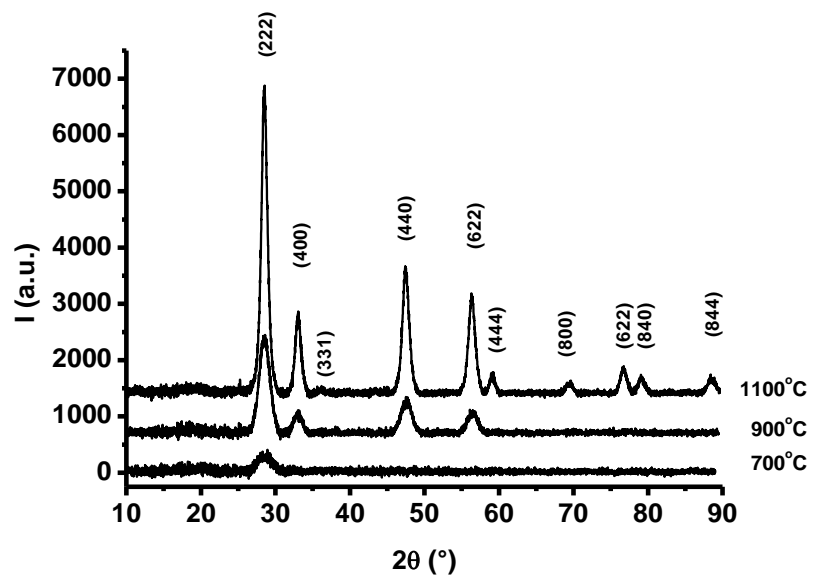
31 Fig. 5 RHEED image of the LZO film which was deposited under optimized conditions.
32
33
34
35

36 Fig.6 C1s by XPS versus sputtering time for samples treated under different Ar-5% H_2 gas
37 flow and at two temperatures.
38
39
40
41
42
43
44
45
46
47
48
49
50
51
52
53
54
55
56
57
58
59
60
61
62
63
64
65

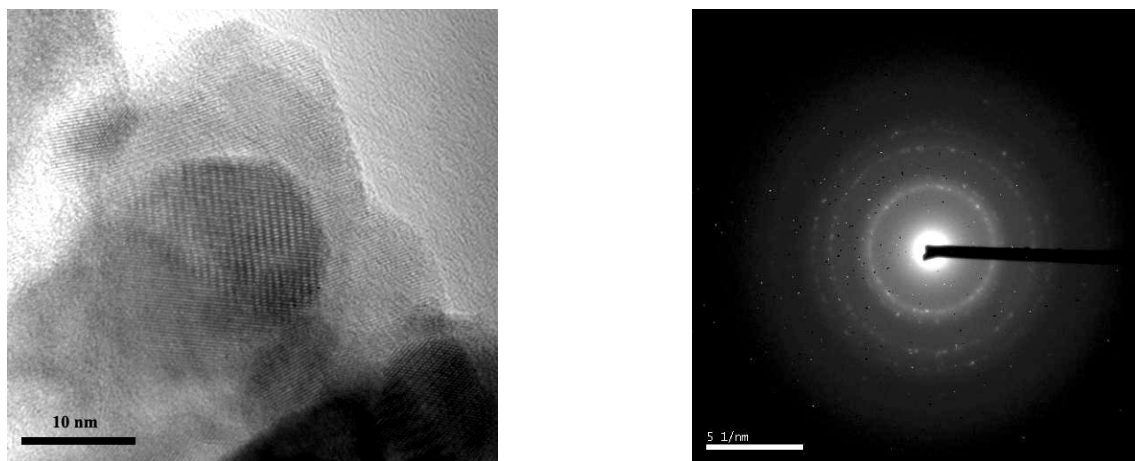
1
2
3
4
5
6
7
8
9
10
11
12
13
14
15
16
17
18
19
20
21
22
23
24
25
26
27
28
29
30
31
32
33
34
35
36
37
38
39
40
41
42
43
44
45
46
47
48
49
50
51
52
53
54
55
56
57
58
59
60
61
62
63
64
65

Fig. 1 Yu et al

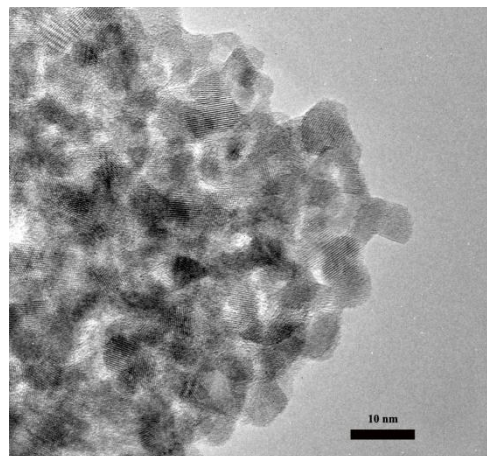
1a)



1b)



1c)



1d)

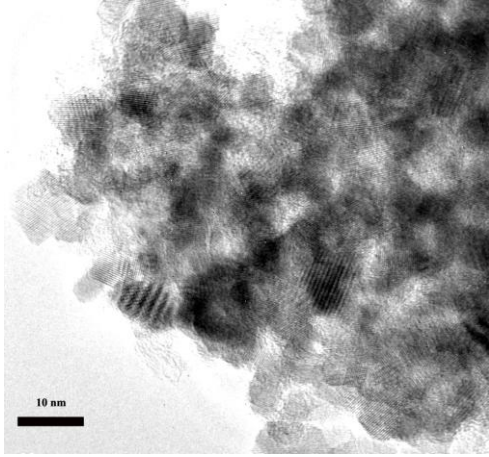
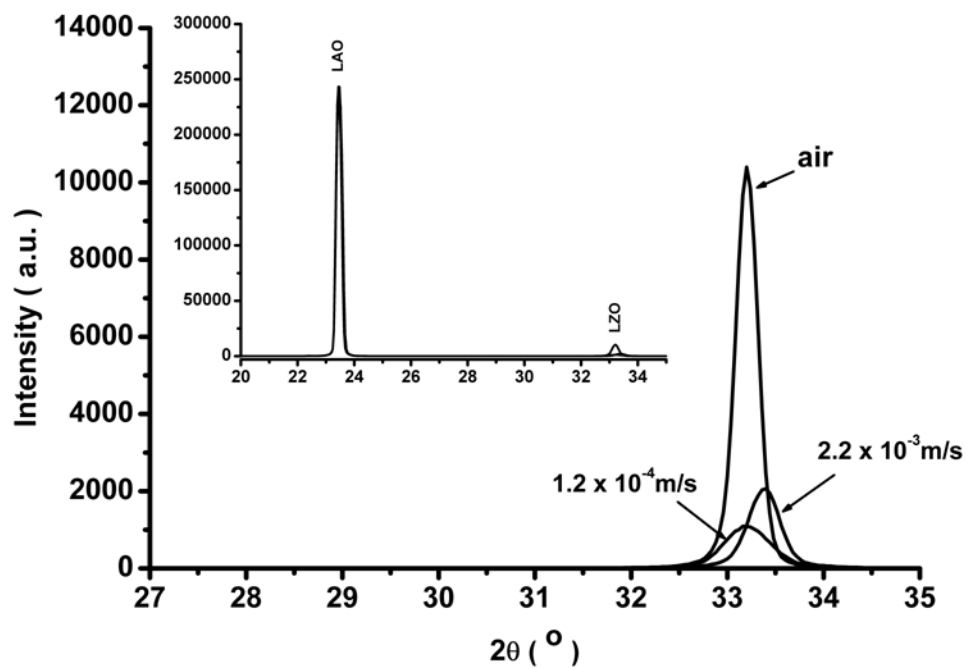


Fig.2

(a)



(b)

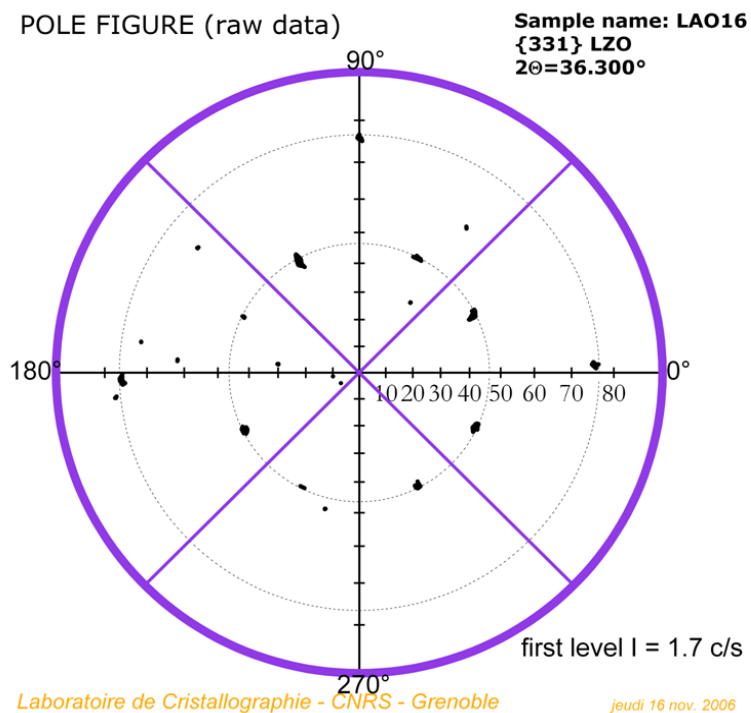


Fig.3

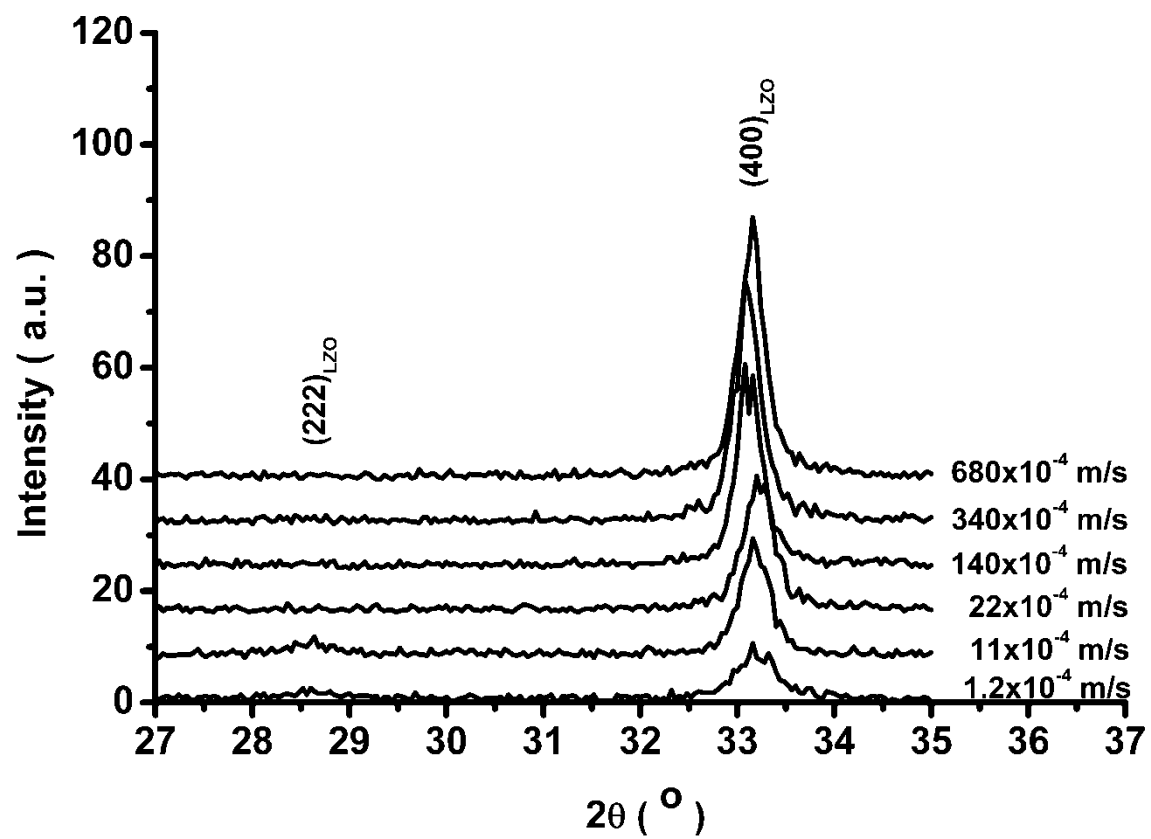
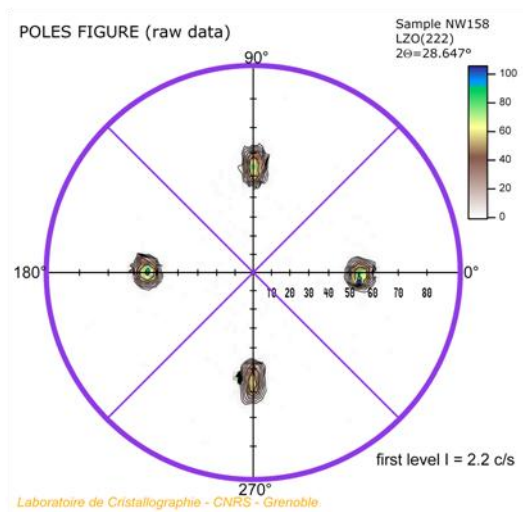
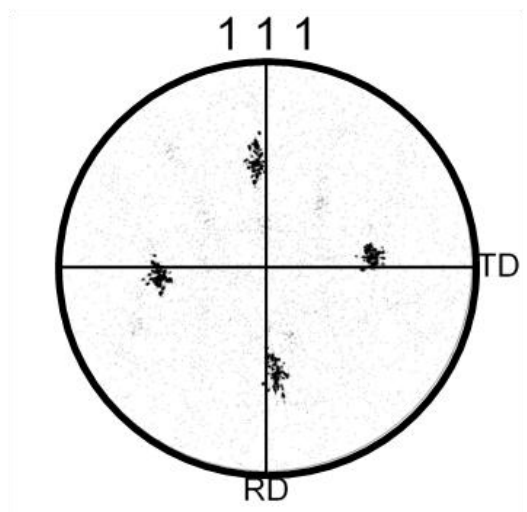


Fig.4 Yu et al



a)



b)

Fig.5 Yu et al

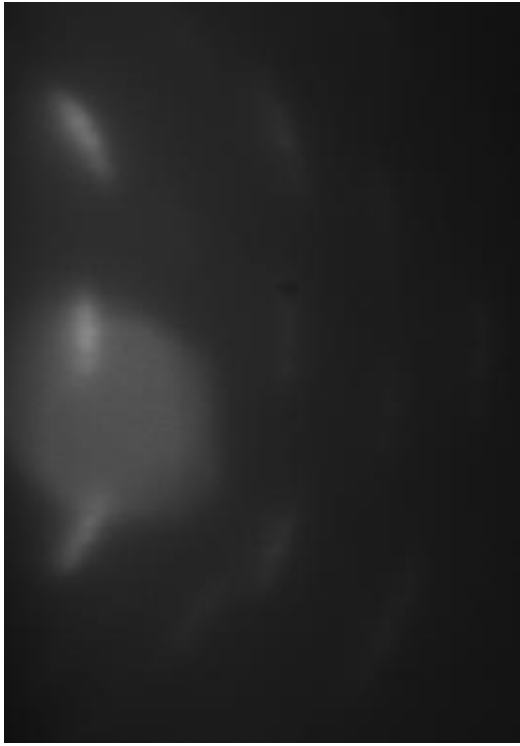


Fig.6

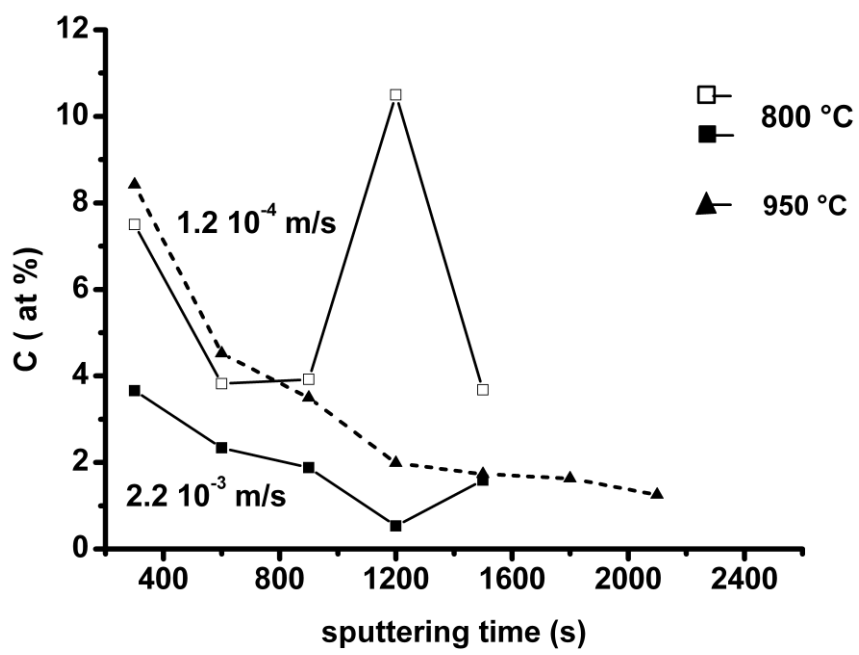


Table 1 Yu et al

Table 1

Temperature	Elements (wt%)				
	C	H	O	La	Zr
<i>propionate</i>	(34)	(4.7)	(30.2)	(18.7)	(12.3)
<i>pentadionate</i>	(45.5)	(5.3)	(20.8)	(15)	(9.9)
as received	33.4	4.8	-----	18.63	11.39
500°C	9.67	-----	-----	-----	-----
700°C	10.7	< 0.3	20.6	40.6	26.92
900°C	11.37	-----	-----	-----	-----
1100°C	11.99	< 0.3	18.92	41.76	25.38

Note: (1) in brackets is the weight fractions calculated from the chemical formula; (2) ----- not determined.